(Received 30 March 2024, Accepted 21 May 2024, Scheduled 4 June 2024)

Design and Optimization of a Circular Ring-Shaped UWB Fractal Antenna for Wireless Multi-Band Applications Using Particle Swarm Optimization

Rania Hamdy Elabd[1, 2] and Ahmed Jamal Abdullah Al-Gburi[3, *]

[1] *Electronic and Communication Department*
Higher Institute of Engineering and Technology in New Damietta, Damietta 34517, Egypt
[2] *Electronic and Communication Department, Horus University, New Damietta, Egypt*
[3] *Center for Telecommunication Research & Innovation (CeTRI), Faculty of Electronics and Computer Technology and Engineering*
Universiti Teknikal Malaysia Melaka (UTeM), Jalan Hang Tuah Jaya, Durian Tunggal, Melaka 76100, Malaysia

ABSTRACT: This study introduces a groundbreaking circular ring-shaped fractal antenna optimized using particle swarm optimization (PSO) for wireless ultra-wideband (UWB) applications. The proposed fractal antenna design, featuring a central plus sign and an outer circular ring with eight smaller rings, enhances bandwidth for UWB response. The ground plane is modified with an etched curved slit to optimize antenna impedance. Utilizing PSO, we determine the fractal antenna's dimensions with optimization goals of minimizing size while ensuring $|S_{11}| < -10$ dB. Experimental data demonstrates strong performance across the 2.05 GHz–14.5 GHz frequency range, covering diverse wireless standards like UWB from 3.1 up to 10.6 GHz, X-band from 8 up to 12.5 GHz, and lower band of Ku from 12.5 to 14.5 GHz. Consistent measured and simulated results validate our contribution's applicability. Additionally, a time-domain analysis underscores the antenna's adaptability to UWB applications, offering insights into its response to transient signals.

1. INTRODUCTION

The wireless communication technology has advanced rapidly in the last few decades, becoming an essential part of our daily lives. The creation of wireless technologies and their broad use have completely changed how we engage with the outside world, communicate, and obtain information. Signals are sent and received wirelessly in a communication system without the need of wires or cables [1].

People may now communicate and obtain information more easily and effectively, at any time and from any location. The multiband functioning among almost unique frequencies with the addition of fractal structure was expected by the wireless communication industry. The self-similar features of fractal geometries led to the development of a novel design approach for small multiband antennas [2].

Broadband antennas are essential components of many wireless communication, radar, and sensor systems. New approaches to wideband antenna design have been made possible by recent advancements in antenna technology [5, 6]. Using multilayer antennas, which stack many layers of conductive and dielectric materials to provide larger bandwidth, is one of the potential ways [7]. Utilizing reconfigurable antennas, which have the ability to change their characteristics in real time to accommodate shifting signal circumstances, is an additional strategy. Switches, adjustable capacitors, and other components that may change the radiation pattern or resonant frequency of the antenna may be used in this method [8, 9].

Because of its high transmission rate, reliability, capacity to resolve multipath components, and simplicity of penetration, UWB technology is popular in the microwave [10–13]. By integrating beam creation, diversity, and multiplexing, UWB is a well-known approach that improves wireless system performance in the face of fading and interference [14–18].

Fractal-type miniaturized antennas have recently attracted more interest from industry professionals as well as academics. It is still difficult to construct an internally compact antenna with a multiband in a tiny phone, nevertheless [19, 20].

The fractal antenna type can overcome the aforementioned difficulties. It may be applied to antennas to reduce size and provide a low profile. The space-filling property and self-similar properties are fractal's two primary features [20]. Space-filling reduces the antenna's size, whereas self-similarity multiplies the original shape's copies with various scaling factors [21, 22]. The antenna may function on several frequencies by using this fractal method to solve the spacing issue. Multiband quality is provided by several fractal structures, such as the Apollonian gasket, Cantor set, Koch, Sierpinski carpet, and Sierpinski gasket [20–24].

In the literature, there are several fractal structures that exhibit multiband properties [1, 23–30]. Monopole antenna configurations are often best suited for narrowband uses. The electromagnetic properties of monopole antennas with fractal structures are reviewed and classified into four main classes: highly

* Corresponding author: Ahmed Jamal Abdullah Al-Gburi (ahmedjamal@ieee.org and engahmed_jamall@yahoo.com).

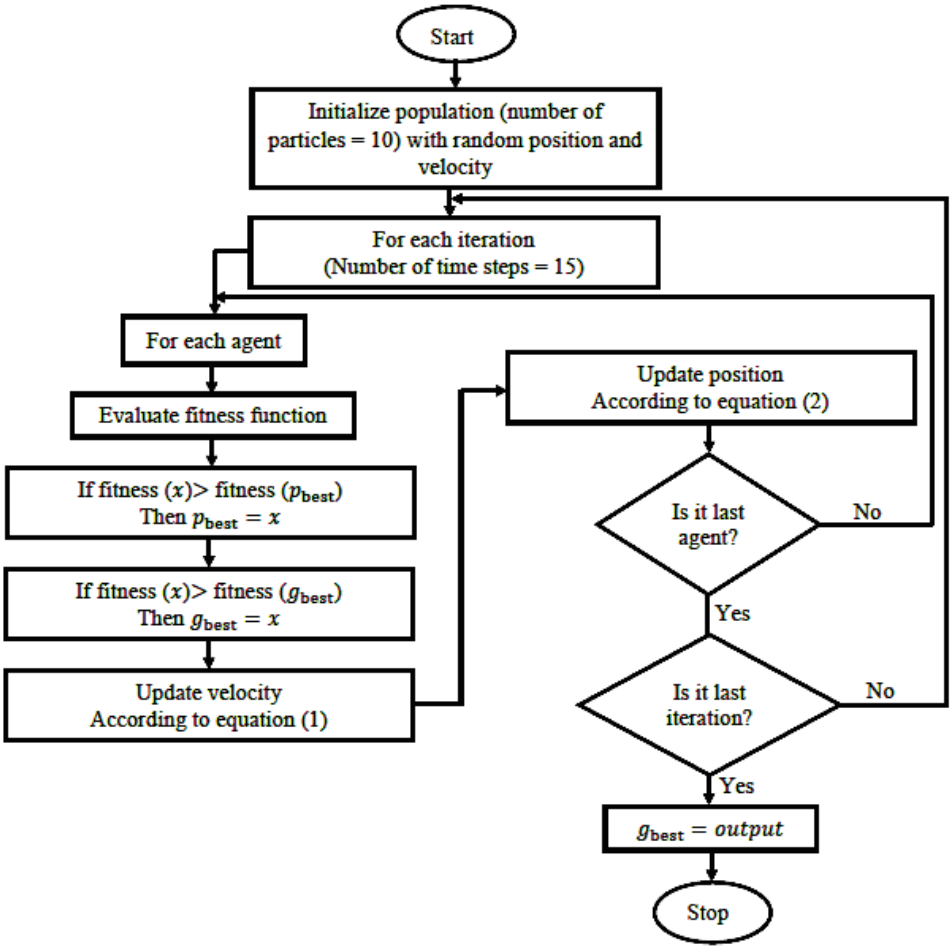

FIGURE 1. Flowchart of the PSO algorithm used for Fractal antenna optimization.

directional, compact and downsized components operating in confined modes, numerous resonances with broadband characteristics, and multi-frequency antennas [24–27]. Within the specified smaller region, the present path lengthens due to the fractal shape [28, 29].

At the moment, a variety of fractal designs have been reported to demonstrate multi-directive radiation capacity in addition to miniaturization. When an electromagnetic wave propagates, a fractal monopole antenna that is polarized in the linear direction generates a narrow beam of radiation [30]. It is more difficult to determine an antenna's precise dimensions in order to obtain an optimal response in a shorter amount of time and lower the antenna design cost [31].

Numerous optimization approaches, such as Genetic Algorithm (GA), Artificial Neural Network (ANN), and Particle Swarm Optimization (PSO), are used in research, engineering, and communication systems. A simple, dependable, and effective method for search and optimization in a variety of EM problems is the PSO. An example of a field full of bees might be used to describe the evolution of PSO. In a field, a swarm of bees looks for the region with the highest density of flowers per square inch. This motivates engineers to use PSO as an optimization technique [32, 33].

The PSO algorithm has garnered significant interest from scholars in the last ten years because of its simple implementation and low number of regulatory parts. PSO is an iterative computer-based approach to problem solving that seeks to enhance a potential solution in accordance with a standard of quality. Compared to GA, PSO converges more quickly [34–36].

PSO's benefits and drawbacks compared to other optimization strategies are thoroughly examined in [37]. PSO is used in [38] to reduce the side-lobe level of the antenna by enhancing the phase distribution of the transmit array. In [39], PSO is used to create the antenna design.

This paper proposes a unique circular ring-shaped fractal antenna for UWB applications. The circular ring-shaped Fractal antenna construction is made up of a circular ring with eight smaller circular rings on the surface of the main ring and a plus sign with a hole in the middle to enhance impedance matching and boost bandwidth. The fractal antenna's bandwidth is increased by mitigating extra capacitive reactance through the usage of this plus sign that couples with the partial ground. The PSO method is used to determine the fractal antenna's dimensions.

The optimization objectives are to minimize the fractal antenna's dimensions within the necessary bandwidth while maintaining the scattering parameter at $|S_{11}| < -10$ dB. With

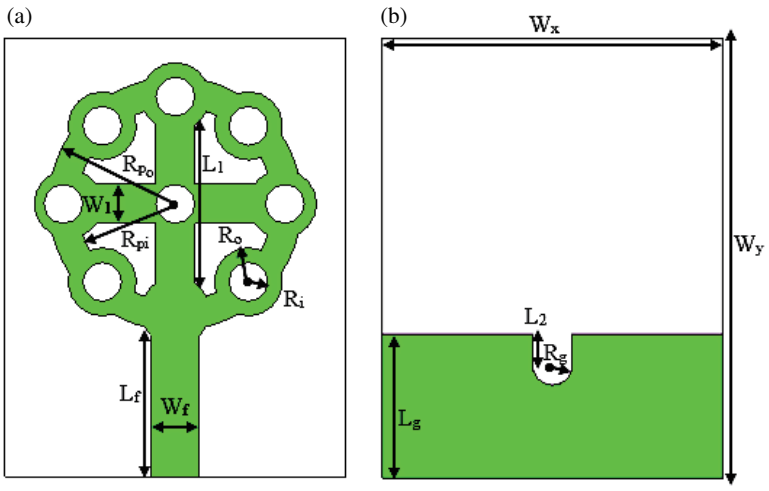

FIGURE 2. The patch antenna's geometry. (a) Top view. (b) Bottom view.

this setup, an 18 GHz broad impedance bandwidth between 2.05 GHz and 14.5 GHz is achieved. Moreover, the antenna remains stable across its whole working range with respect to radiation and input impedance. It is appropriate for UWB frequencies from 3.1 up to 10.6 GHz, X-band from 8 up to 12.5 GHz, and lower band of Ku from 12.5 to 14.5 GHz.

2. PARTICLE SWARM OPTIMIZATION ALGORITHM

To ensure that the study is comprehensive, a brief description of the step-by-step algorithm is provided, along with the flowchart seen in Figure 1.

To facilitate a better understanding of the implementation process for optimizing the required band and, consequently, extracting the structural characteristics of a circular ring-shaped Fractal antenna, as detailed in the upcoming section, the PSO method is provided below. The detailed process is provided after that.

Step 1: Identify the space of solutions. In this area, the parameters that need to be optimized are chosen. N is the dimension of the optimization space, and n runs from 1 to N. A minimal range $(x_{\min(n)})$ and a maximum range $(x_{\max(n)})$ are specified.

Step 2: Identify a fitness function. There is a functional reliance of the fitness function on the significance of each attribute under optimization.

Step 3: Set the swarm's initial random location and velocities. Every particle starts at a random place and moves at a random speed, both in terms of direction and magnitude. There is a global best (g_{best}) and a personal best (p_{best}). The position with the greatest fitness level locally is the personal best; the position with the highest fitness level across the board is the global best.

Step 4: Fly the particles throughout the solution space in a methodical manner. The program cycles across the whole swarm, moving each particle a tiny distance at a time. Every particle encounters the subsequent phases. g_{best} and p_{best} are used to compare the particle's fitness. The following equation is used to update the particle's velocity further based on the fitness value:

$$v_n = w{*}v_n{+}C_1{*}r_1\left(p_{best,n} - x_n\right){+}C_2{*}r_2(g_{best,n}{-}x_n) \quad (1)$$

where C_1 and C_2 are two scaling factors that determine the relative pull of p_{best} and g_{best}, and r_1, r_2 are random variables in the range [0, 1]. W is known as inertial weight (range is between 0.0 and 1.0), and x_n, v_n are the particle's coordinate and velocity in the n^{th} dimension, respectively.

1. The particle must go to its next destination when its velocity has been changed. The velocity is applied per time-step t, and the following equation is used to determine the new coordinate x_n for each of the N dimensions:

$$x_n = x_n + \Delta t * vn \quad (2)$$

Step 5: Repeat Step 4 for every particle in the swarm. The complete swarm's picture is taken once per second, at which point all particle locations are assessed, and if necessary, adjustments are made to the values of p_{best} and g_{best}.

2.1. Implementation of PSO

Equation (3) indicates that the fitness function $|S_{11}|$ in the chosen band must be smaller than -10 dB. The inertia weight (w) in our design is 1. The value of C_1 and C_2 is 2. For the given swarm size, the maximum number of solver evaluations is 451, and the maximum number of iterations is 15. The optimization equation is:

$$S_{11}(f) = -20 * \log|\Gamma|, \quad |\Gamma| \leq 1 \quad (3)$$

$$\Gamma = \frac{Z_{in} - Z_o}{Z_{in} + Z_o} \quad (4)$$

where f denotes the frequency, $f \in (2.05, 14.5)$ GHz, Γ the reflection coefficient of the antenna, Z_o the characteristics of the coaxial feed, the antenna's output impedance of 50 Ω for matching, and Z_{in} the input impedance of the antenna.

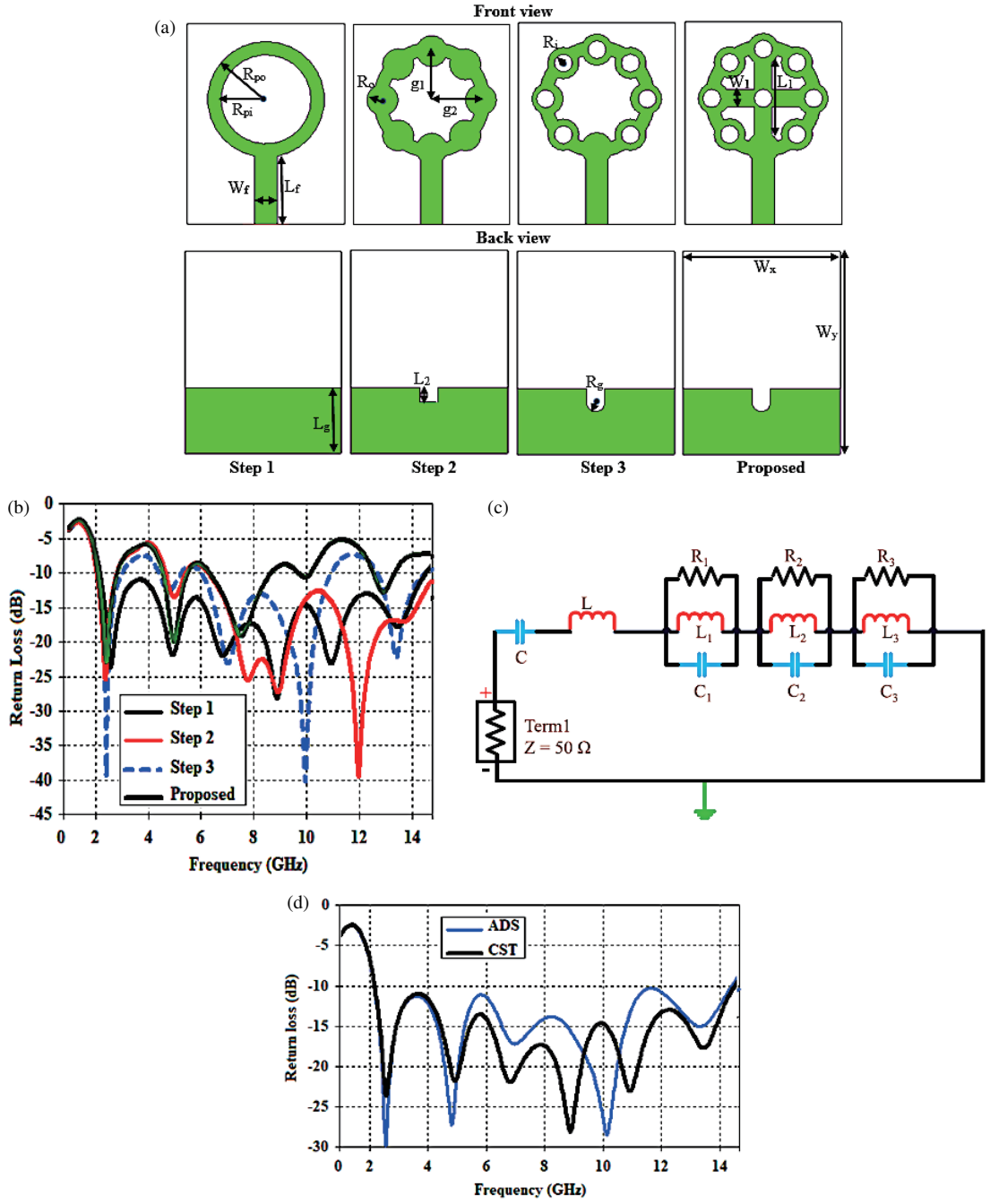

FIGURE 3. (a) Phases of the planned fractal antenna's progressive design. (b) Reflection Coefficient (S_{11} (dB)), (c) equivalent circuit of the UWB antenna. And (d) ADS and CST outcomes.

3. ANTENNA DESIGN AND CONFIGURATION

The suggested circular ring-shaped fractal antenna is shown in Figure 2; it was created on a Roger RT5880 substrate with a loss tangent of 0.0009 and a dielectric constant of ε_r of 2.2 using a CST simulator. The thickness of the substrate is 1.75 mm. The circular ring-shaped fractal antenna construction is made up of a circular ring with eight smaller circular rings on its surface and a plus sign with a hole in the center to expand its bandwidth located in the center of the main ring. The fractal antenna's bandwidth is increased by mitigating extra capacitive reactance through the usage of this plus sign that couples with the partial ground. The printed suggested fractal antenna with partly ground dimensions is $38 \times 45\,\text{mm}^2$.

The step-by-step approach of creating an antenna patch is depicted in Figure 3(a). The circular radiating patch is first designed as a circular ring structure by removing the circle of radius R_{pi} from it. Equations (5) and (6) [35] are used to determine the circular patch's radius, and Figure 3(b) plots the corresponding reflection coefficient $|S_{11}|$.

$$R_{po} = \frac{F}{\sqrt{1 + \left(\frac{2h}{\pi\varepsilon_r F}\right)\left[\ln\left(\frac{\pi F}{2h}\right) + 1.7726\right]}} \tag{5}$$

TABLE 1. Optimized parameters of the proposed fractal antenna using PSO in (Millimeters).

W_x	W_y	R_{po}	R_{pi}	L_f	W_f	R_i	R_o	L_1	W_1	L_g	L_2	R_g	g_1	g_2
38	45	14.3	11.3	16	5.47	2	3.5	16.3	4	14.7	3	2	12.8	12.8

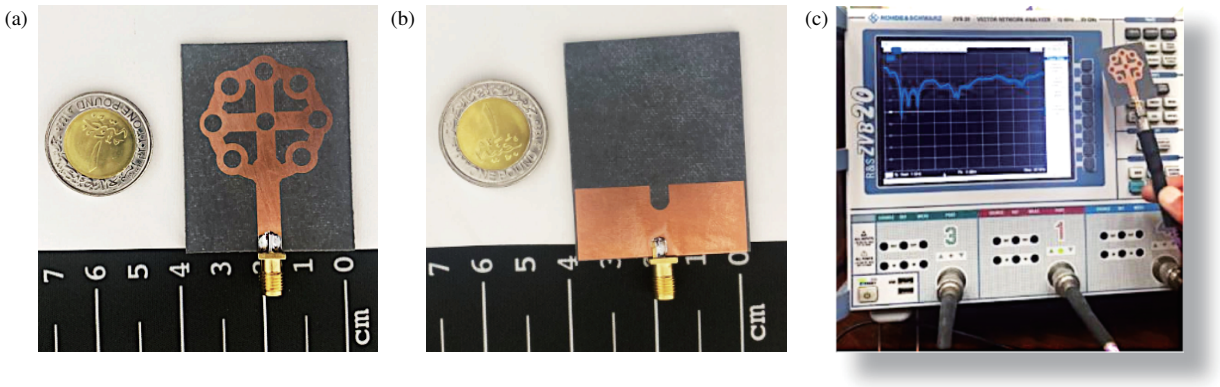

FIGURE 4. The manufactured prototype of the planned antenna is depicted along with the corresponding measurements: (a) presents the front view, (b) showcases the back view, and (c) illustrates the S11 measurement setup using a VNA.

$$F = \frac{8.791 \times 10^9}{f_r\sqrt{\varepsilon}_r} \tag{6}$$

The first step design is seen to be functioning in a number of narrow bands. As shown in the second stage, 8 circles are added to the ring patch's surface in order to increase impedance matching and achieve resonance in the UWB spectrum. As seen in Figure 3(b), the addition of more circles tends to produce UWB response from 2.05 to 3 GHz and from 6 to 11 GHz.

As seen in Figure 3(a), seven holes were etched into seven of the eight circles that were created in the previous phase in the third step. As seen in Figure 3(b), the addition of etched holes often results in UWB response and enhances impedance matching. As seen in the suggested fractal antenna, further impedance matching is achieved by creating a curved slit in the partial ground plane and adding a plus singe to the center of the main ring with hole, with the corresponding S_{11} displayed in Figure 3(b). The design and simulation procedures are carried out using CST Microwave Studio v2019.

Equations (5) and (6) yield the fractal antenna's dimensions, which are the starting points for the PSO algorithm.

The constraints on the dimensions of the proposed Fractal antenna are as follows: R_{po} ranges from 13 to 15.6 mm; R_{pi} ranges from 10 to 13 mm; L_f ranges from 14 to 17 mm; R_o ranges from 2.7 to 4.2 mm; R_i ranges from 1 to 3 mm; R_g ranges from 2 to 4 mm; and L_g ranges from 14.2 to 15.5 mm, in which $2 * R_{po} < W_x$, $2 * R_{po} < W_y - L_f$, $L_g < L_f$.

The radius of the radiating disc is denoted by R_{po}; the thickness of the Roger RT 5880 substrate is h; the effective permittivity is represented by ε_r; and the center frequency is f_r. Table 1 is a list of the Fractal antenna's geometric specifications. The manufactured circular ring-shaped fractal antenna is seen in Figure 4.

The frequency ranges 2.05 GHz–14.5 GHz are covered by this system. The aforementioned frequency ranges correspond to specific wireless standards, including UWB from 3.1 up to 10.6 GHz, X-band from 8 up to 12.5 GHz, and lower band of Ku from 12.5 to 14.5 GHz. In order to get a broad bandwidth, the dimensions of the fractal antenna are determined in this research using particle swarm analysis. An analogous circuit model was created in the advanced design system (ADS) program in order to understand the ultra-wideband antenna's wideband properties, as shown in Figure 3(c). The degeneration Foster canonical (DFC) model, which is commonly used for characterizing ultra-wideband antennas, forms the foundation of this circuit. When an antenna exhibits wideband features, it may be seen as a radiating element that generates several closely spaced resonances, wherein some neighboring bands cross over [46, 47]. As seen in Figure 3(d), the ideal simulation and similar circuit's simulation results are contrasted. Parallel connections between RLC lumped elements allow for the analysis of each resonance band. Numerous parallel-connected RLC circuits with narrowly spaced bands can be coupled in series to provide a wideband characteristic. Figure 3(c) shows the capacitance and inductance, respectively, represented by letters C and L, when the ultra-wideband antenna is resonating at the fundamental lower mode. The remaining higher resonances are realized by the three parallel RLC circuits coupled in series. The radiation resistances of the associated resonances are represented by three resistors, $R1$, $R2$, and $R3$. The impedance matching inside the operating band is controlled by the left RLC circuit, which consists of $R1$, $C1$, and $L1$. The lower side of the ultra-wideband is adjusted by the center RLC tank, which consists of $R2$, $C2$, and $L2$. The upper frequencies are controlled by the right RLC circuit, which consists of $R3$, $C3$, and $L3$. Table 2 provides the values of the electrical components used in the analogous circuit.

TABLE 2. The values of the electrical components utilized in the circuit correspond to each other.

C	L	R_1	L_1	C_1	R_2	L_2	C_2	R_3	L_3	C_3
1.32 pF	4.52 nH	32 Ω	2.473 nH	4 pF	2.41 Ω	2.24 nH	3.2 pF	82.9 Ω	1.29 nH	0.695 pF

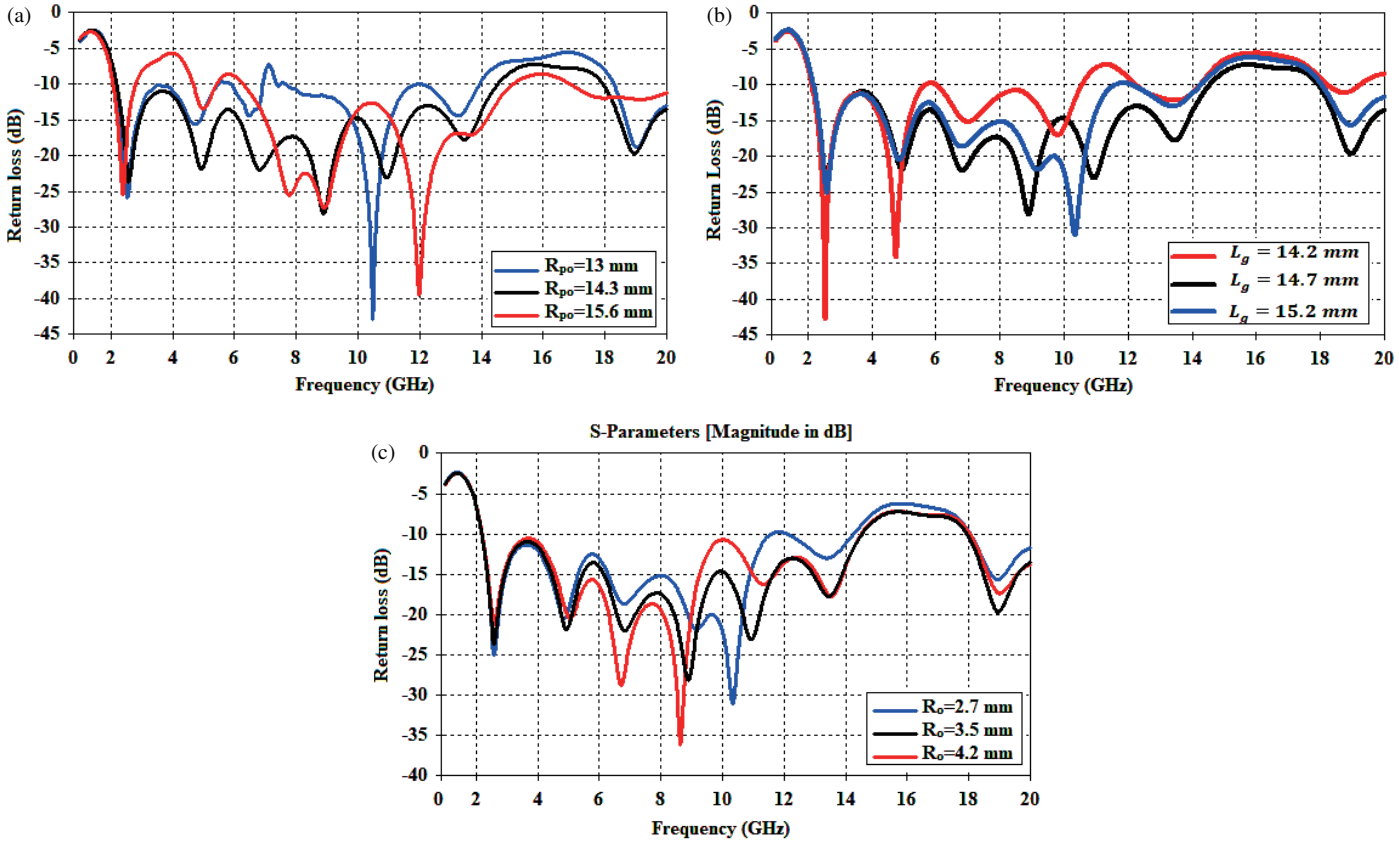

FIGURE 5. Reflection coefficient simulation for the suggested fractal antenna with several values of (a) R_{op}, (b) R_o and (c) L_g.

TABLE 3. Comparison of proposed UWB antennas intended for biomedical and Multiband applications with previously demonstrated.

Ref.	Dimensions mm^2	Dielectric material	ε_r	Frequency band (GHz)	Efficiency (%)	Gain (dBi)
[3]	25 × 35	RT/Duroid 5880	2.2	3.2–20	85	5.36
[41]	24 × 30	FR-4	4.4	1.0–2.75 4.74–8.70 11.04–12.76 14.97–16.62 19.70–22.0	NA	3.37
[42]	14.9 × 33.14	FR-4	4.4	3-11	NA	4.74
[43]	50 × 60	Denim substrate	1.4	7–28	90	10.1
[44]	29 × 27	FR-4	4.4	3–15	NA	NA
[45]	19 × 21	FR-4	4.4	3–13.5	NA	4
[46]	20 × 28	FR-4	4.4	2.95–12	85	4
[47]	27 × 50	FR-4	4.4	1.63–1.88 4.5–8.5	90	5.5
[48]	34 × 30	FR-4	4.3	3.2–7.5	91	2
Proposed	**38 × 45**	**Roger RT5880**	**2.2**	**2.05 GHz–14.5 GHz**	**95**	**6**

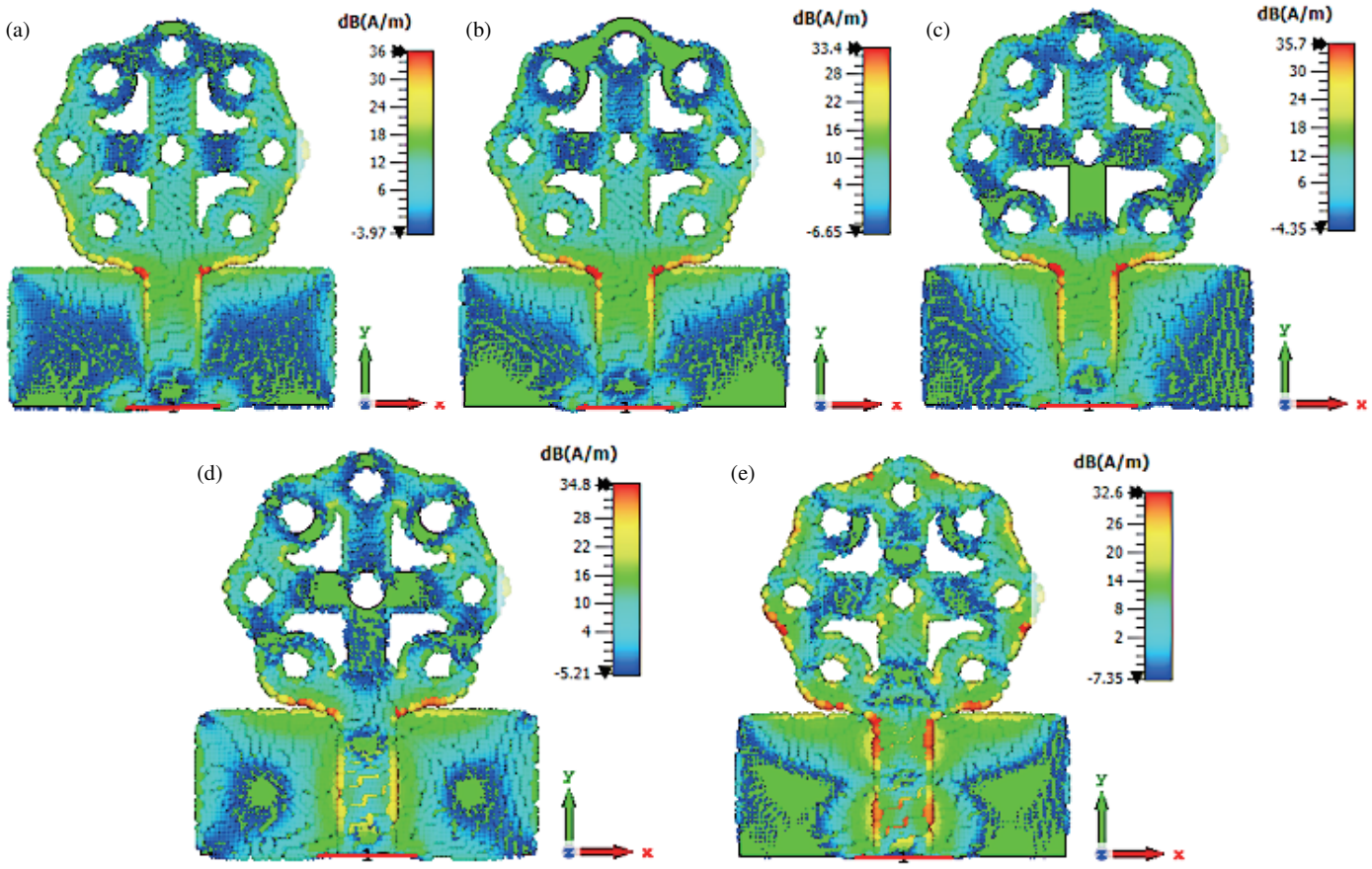

FIGURE 6. Surface current distribution on the proposed antenna's radiating patch. (a) 2.4 GHz, (b) 3.3 GHz, (c) 4.5 GHz, (d) 8 GHz, (e) 12 GHz.

4. RESULTS AND DISCUSSION

As seen in Figure 4, the suggested antenna is manufactured by photolithography and simulated using the commercial CST 2019. A Roger RT5880 material substrate with a loss tangent of 0.0009 and a dielectric constant ε_r of 2.2 is used. The thickness of the substrate is 1.75 mm.

By placing restrictions on an antenna's dimensions as the lowest and maximum values of the generated antenna's dimensions are set, the optimization aims are to obtain the smallest dimensions of the antenna in the desired bandwidth while maintaining $|S_{11}|$ below -10 dB. As seen in Figure 5, the radius of the Fractal antenna is the primary factor that determines its center frequency.

As Figure 5 shows, we observe that the antenna's bandwidth is determined by the patch's radius. Greater bandwidth is located at $L_g = 14.7$ mm, $R_{op} = 14.3$ mm, and $R_o = 3.5$ mm. Figure 6 displays the associated surface current distribution of the suggested fractal antenna for frequencies of 2.4 GHz, 3.3 GHz, 4.5 GHz, 8 GHz, and 12 GHz, and shows that the transmission feed line and fractal radiating patch get most of the current. The currents are shown to be more densely packed toward the fractal antenna's surface. Consequently, the bandwidth will be broadened as a result of these currents.

The simulated and observed reflection coefficients are shown in Figure 7(a). One is the applied inertia weight. In addition to increasing the antenna's dimensions as seen in Figure 7(b), changing the inertia weight to 0.5 boosts bandwidth at the cost of a tangential return loss to -10 dB, which cannot be guaranteed in fabrication.

Within the necessary bandwidth, the antenna may produce -10 dB to -25 dB, according to the observed findings of $|S_{11}|$. The frequency range that the antenna can cover is 2.05 GHz–14.5 GHz.

The obtained impedance bandwidths are sufficiently large to accommodate various wireless standards, including those covered by UWB from 3.1 up to 10.6 GHz, X-band from 8 up to 12.5 GHz, and lower band of Ku from 12.5 to 14.5 GHz.

By using the PSO method, we may reduce the antenna's dimensions to the minimum while maintaining the necessary bandwidth without raising the cost of manufacturing due to larger dimensions. The final antenna dimensions were provided in less time since this method of constructing an antenna without trial and error to obtain the desired bandwidth, high gain, and high efficiency is faster. As seen in Figures 7(c) and (d), respectively, the efficiency varies about 95% while the gain ranges from 2 to 6.5 dBi.

The two-dimensional (2D) radiation patterns for the E- and H-planes are shown in Figure 8. We calculated the radiation characteristics for the following frequency bands: 2.4, 3.3, 4.5, 8, and 12 GHz. The antenna possesses omnidirectional capa-

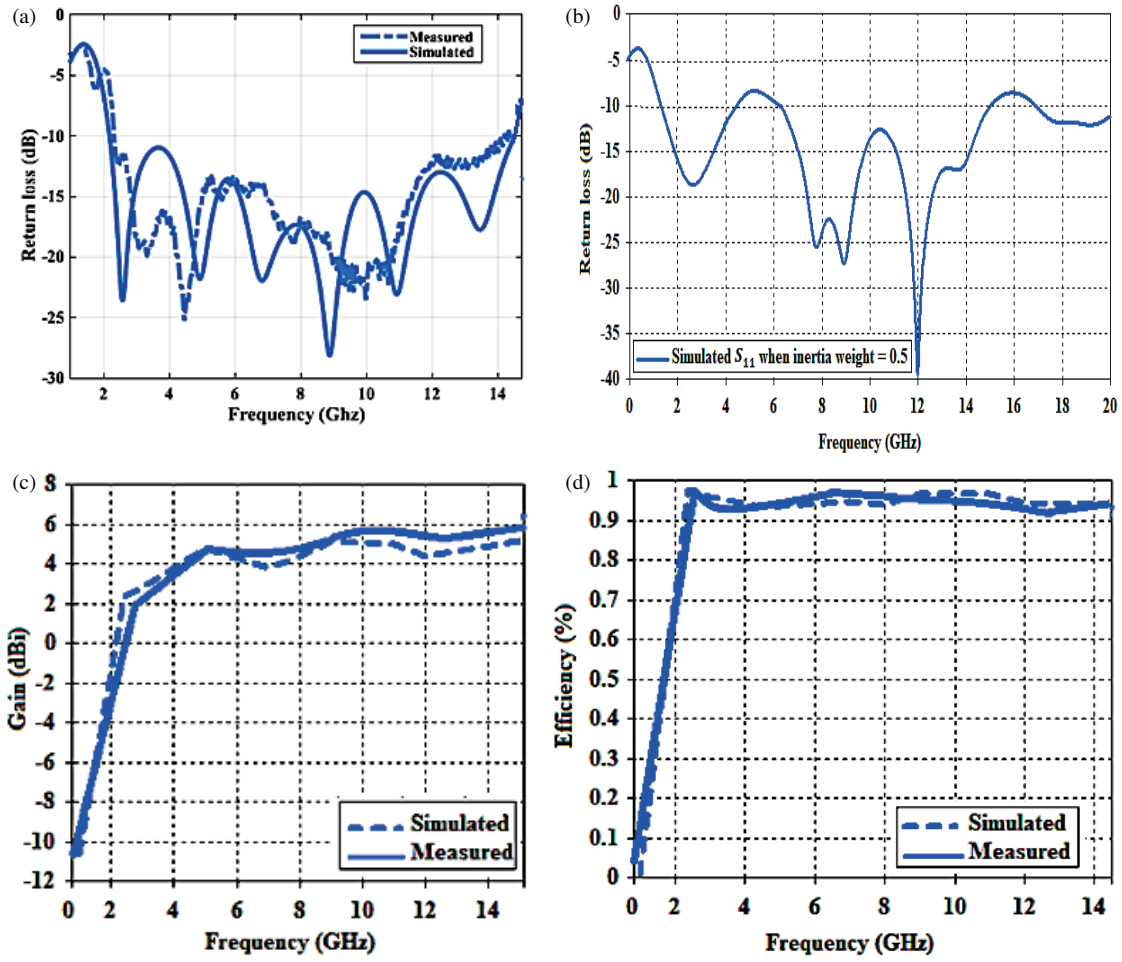

FIGURE 7. The measured and simulated parameters of proposed fractal antenna. (a) Return loss. (b) Simulated return loss when inertia weight = 0.5. (c) Gain and (d) Efficiency.

bilities for the H-plane and bidirectional properties for the E-plane, as seen in Figure 8. Additionally, the provided antenna exhibits nearly consistent response across the operational bandwidth, demonstrating outstanding coverage.

4.1. Analysis of the Antenna's Performance in the Time Domain

For near-field microwave medical imaging applications, it is critical to assess the antenna's performance in the temporal domain [3, 13], taking into account factors such as the forward transmission coefficient (S_{21}), S_{21} phase, and group delay. This means that two identical antennas are placed side by side and face to face with a distance of 30 cm between them. Figures 9(a) and 9(b) show this configuration with both antennas in transceiver mode.

Antennas are excited by a Gaussian pulse with an operating range of 1–20 GHz in order to assess the time-domain performance of the suggested antenna. Figures 10(a) and 10(b) display the normalized amplitudes of the input and output signals for each configuration. The fidelity factor (FF), or cross-correlation between broadcast and received pulses, is computed using the following formula [40]:

$$FF = \max\left[\frac{\int_{-\infty}^{\infty} S_t(t)S_r(t+\tau)d\tau}{\int_{-\infty}^{\infty}|S_t(t)|^2\,dt\int_{-\infty}^{\infty}|S_r(t)|^2\,dt}\right] \quad (7)$$

In this case, $S_t(t)$ stands for the transmitted signal, $S_r(t)$ for the received signal, and τ denotes the group delay. The face-to-face and side-by-side arrangements have FF values of 82% and 76.85%, respectively. The FF value is high in a face-to-face setup, indicating less distortion in the transmitted signal. Minimal distortion throughout the whole UWB spectrum is sought for UWB antennas. The average delay between the input signal and transient output center is assessed to determine the phase distortion and dispersion properties of an antenna; this phenomenon is called group delay.

The group delay, S_{21} phases, and S_{21} magnitudes are displayed in Figure 1. Figure 10(c) makes it evident that the side-by-side and face-to-side antenna configurations have an S_{21} value lower than -25 dB over the whole range. In Figure 10(d), the S_{21} phase is also displayed to help understand the linearity characteristics within the intended band operation. It is clear from the phase curves that the antenna behaves linearly in the

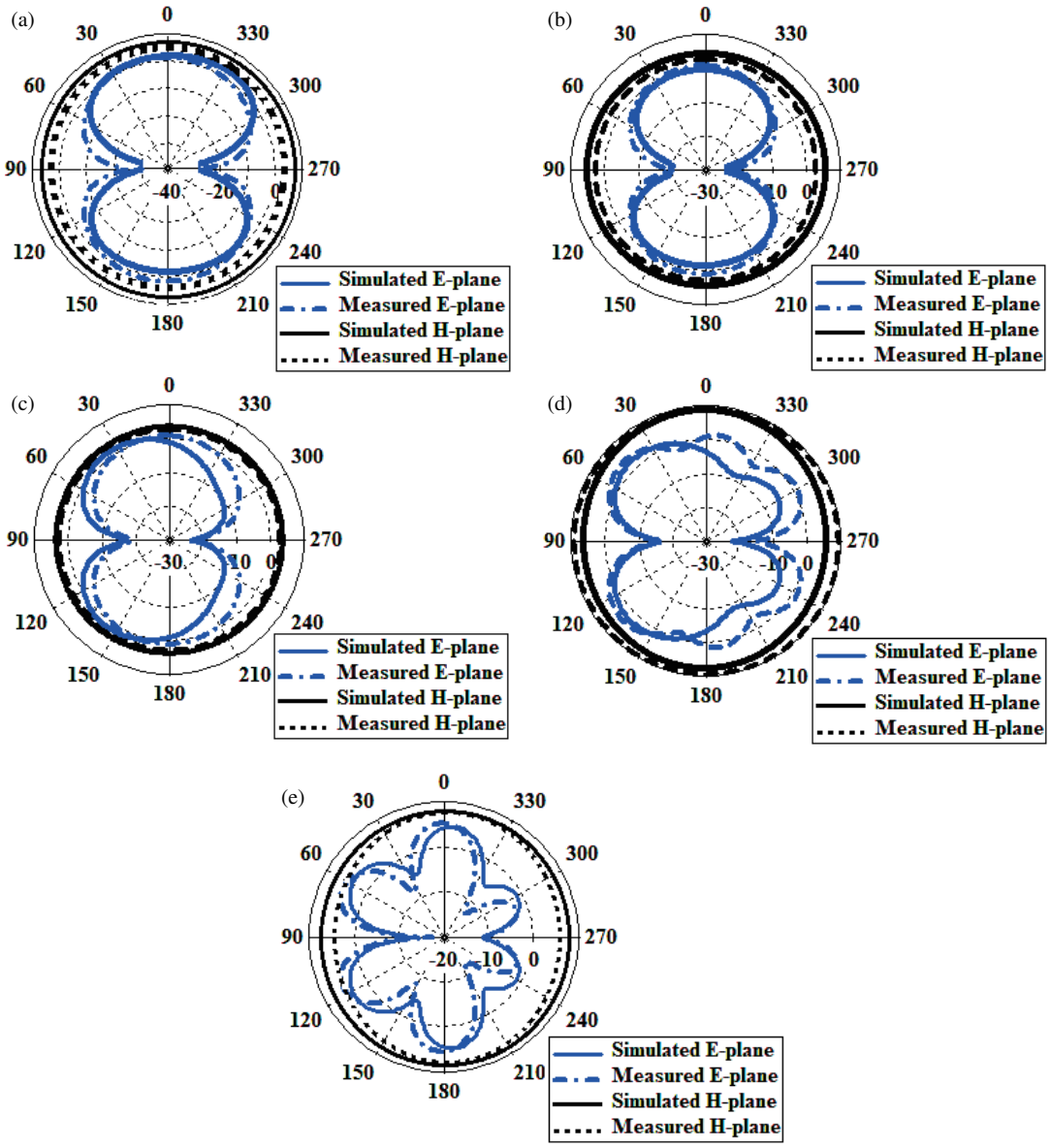

FIGURE 8. Patterns of radiation for the suggested fractal antenna. (a) 2.4 GHz, (b) 3.3 GHz, (c) 4.5 GHz, (d) 8 GHz, (e) 12 GHz.

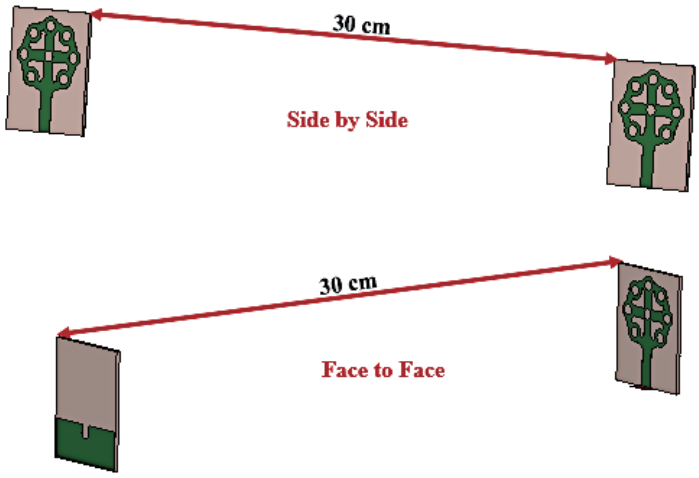

FIGURE 9. Configuration for time-domain analysis in different simulation setups.

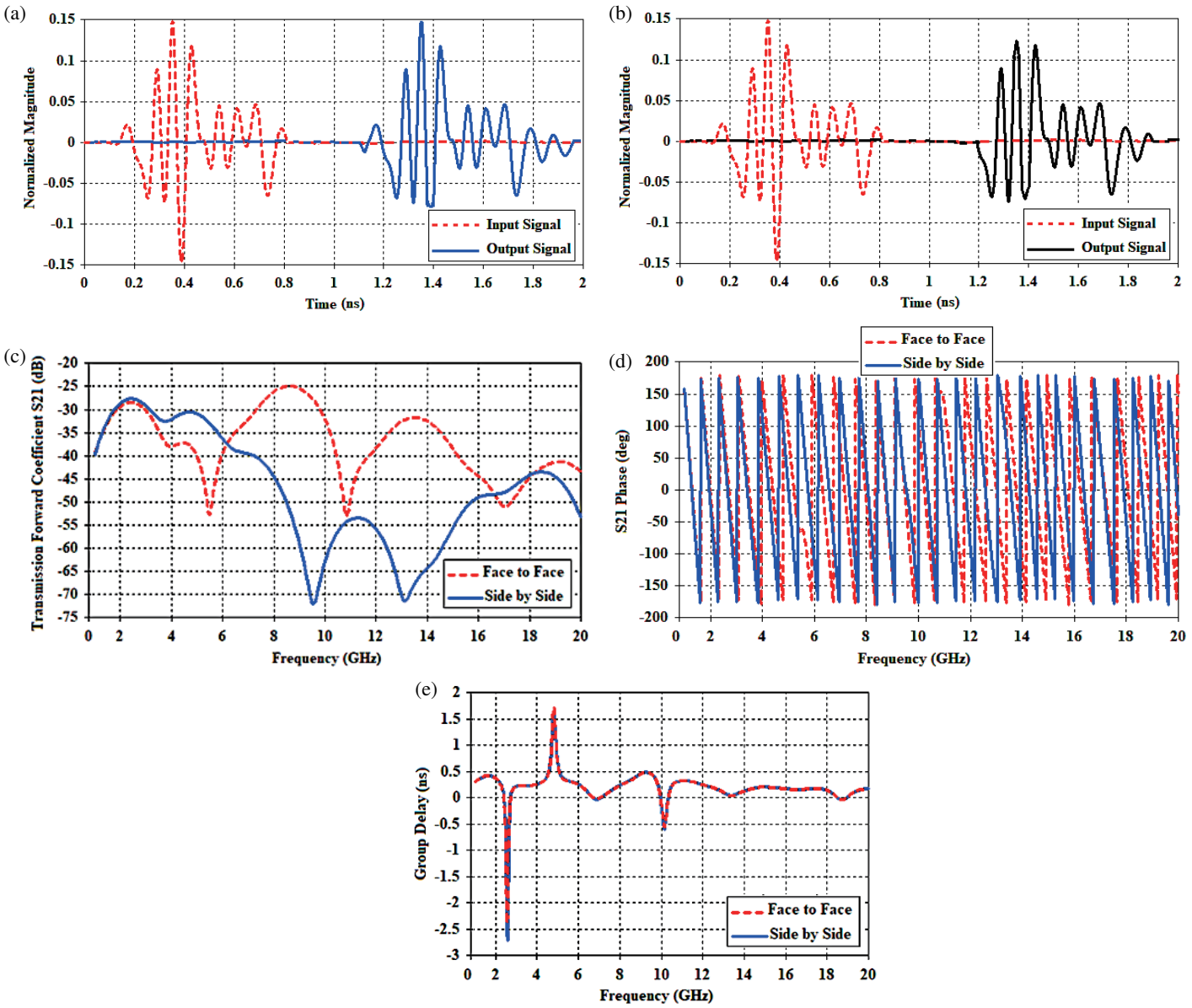

FIGURE 10. Time Domain Performance Analysis of the suggested Antenna. (a) Input and output signals for side by side. (b) Input and output signals for face to face. (c) Transmission forward coefficient. (d) S_{21} phase, and (e) group delay.

desired frequency range in a variety of orientations. Figure 10(e) shows that the peak values of 1.55 ns for both face-to-face and side-by-side arrangements suggest that there will be less distortion when transmitting brief pulses.

5. COMPARISON WITH RELATED WORKS

A thorough comparison of the several antennas intended for UWB applications is provided in Table 3. Dimensions, dielectric material ε_r, operating frequency, fractional bandwidth (FBW), and gain are all included in the comparison. A deeper look reveals that the suggested antenna design has a broad 18 GHz frequency bandwidth, suggesting that it may be used for a variety of UWB spectrum applications. The suggested design is successful in both signal reception and transmission, as evidenced by a significant gain of 6 dBi and FBW of 144.82%. This makes it a viable option for biomedical applications where dependable and efficient signal transmission is crucial.

6. CONCLUSION

We have successfully designed and presented a circular ring-shaped fractal UWB antenna tailored for UWB applications. The radiating element features a central circular ring embellished with eight smaller circular rings and a plus sign with a central hole, strategically employed to expand the bandwidth within the main ring. To further improve impedance matching, a curved slit is intricately etched onto the ground plane. The PSO method has been employed to determine the dimensions of the circular ring-shaped fractal antenna. The optimization objectives prioritize minimizing the antenna's dimensions within the necessary bandwidth, while concurrently adhering to spe-

cific performance criteria: a reflection coefficient (S11) of less than −10 dB, a gain exceeding 6 dBi, and an efficiency of approximately 95%. The impedance of the fractal antenna covers a frequency range from 2.05 to 14.5 GHz. With a broad spectrum coverage, our antenna covers various wireless standards including UWB from 3.1 up to 10.6 GHz, X-band from 8 up to 12.5 GHz, and lower band of Ku from 12.5 to 14.5 GHz. Furthermore, our antenna design exhibits consistent radiation properties across its operational bandwidth. The assessment of the antenna's time-domain performance highlights favorable properties suitable for a variety of biomedical applications, particularly in the realms of microwave and millimeter-wave medical imaging. This holistic approach to design and performance ensures the antenna's applicability and effectiveness in diverse UWB scenarios.

ACKNOWLEDGEMENT

The authors would like to express their gratitude and acknowledge the support received from Universiti Teknikal Malaysia Melaka (UTeM), the Centre for Research and Innovation Management (CRIM), and the Ministry of Higher Education of Malaysia (MOHE).

REFERENCES

[1] Marzouk, M., I. H. Nejdi, R. Youssef, S. Barua, S. Mohamed, S. Ahmad, and M. Hussein, "Efficient broadband fractal antenna for WiMAX and WLAN," *Heliyon*, Vol. 10, 2024.

[2] Manikandan, P. and P. Sivakumar, "A novel pinwheel fractal multiband antenna design using particle swarm optimization for wireless applications," *International Journal of Communication Systems*, Vol. 34, No. 15, e4933, 2021.

[3] Saleem, I., U. Rafique, S. Agarwal, H. S. Savci, S. M. Abbas, and S. Mukhopadhyay, "Ultra-wideband fractal ring antenna for biomedical applications," *International Journal of Antennas and Propagation*, Vol. 2023, Article ID 5515263, 2023.

[4] Mohanraj, P. and P. R. Selvakumaran, "Compact wideband implantable antenna for biomedical applications," *Current Applied Physics*, Vol. 43, 50–56, 2022.

[5] Al-Gburi, A. J. A., M. M. Ismail, N. J. Mohammed, and T. A. H. Alghamdi, "SAR flexible antenna advancements: highly conductive polymer-graphene oxide-silver nanocomposites," *Progress In Electromagnetics Research M*, Vol. 127, 23–30, 2024.

[6] Al-Gburi, A. J. A., M. M. Ismail, N. J. Mohammed, A. Buragohain, and K. Alhassoon, "Electrical conductivity and morphological observation of hybrid filler: silver-graphene oxide nanocomposites for wearable antenna," *Optical Materials*, Vol. 148, 114882, 2024.

[7] Kaur, M., H. S. Singh, and M. Agarwal, "A compact two-state pattern reconfigurable antenna for 5G Sub-6 GHz cellular applications," *AEU — International Journal of Electronics and Communications*, Vol. 162, 154577, 2023.

[8] Nie, Z., H. Zhai, L. Liu, J. Li, D. Hu, and J. Shi, "A dual-polarized frequency-reconfigurable low-profile antenna with harmonic suppression for 5G application," *IEEE Antennas and Wireless Propagation Letters*, Vol. 18, No. 6, 1228–1232, 2019.

[9] Nejdi, I. H., S. Das, Y. Rhazi, B. T. P. Madhav, S. Bri, and M. Aitlafkih, "A compact planar multi-resonant multi-broadband fractal monopole antenna for Wi-Fi, WLAN, Wi-MAX, Bluetooth, LTE, S, C, and X band wireless communication systems," *Journal of Circuits, Systems and Computers*, Vol. 31, No. 11, 2250204, 2022.

[10] Zerrad, F.-e., M. Taouzari, E. M. Makroum, J. E. Aoufi, S. D. Qanadli, M. Karaaslan, A. J. A. Al-Gburi, and Z. Zakaria, "Microwave imaging approach for breast cancer detection using a tapered slot antenna loaded with parasitic components," *Materials*, Vol. 16, No. 4, 1496, 2023.

[11] Sasikala, S., K. Karthika, S. Arunkumar, K. Anusha, S. Adithya, and A. J. A. Al-Gburi, "Design and analysis of a low-profile tapered slot UWB vivaldi antenna for breast cancer diagnosis," *Progress In Electromagnetics Research M*, Vol. 124, 43–51, 2024.

[12] Al-Gburi, A. J. A., I. Ibrahim, Z. Zakaria, and A. D. Khaleel, "Bandwidth and gain enhancement of ultra-wideband monopole antenna using MEBG structure," *ARPN Journal of Engineering and Applied Sciences (JEAS)*, Vol. 14, No. 10, 3390–3393, 2019.

[13] Elabd, R. H., H. H. Abdullah, and M. Abdelazim, "Compact highly directive MIMO vivaldi antenna for 5G millimeter-wave base station," *Journal of Infrared, Millimeter, and Terahertz Waves*, Vol. 42, No. 2, 173–194, 2021.

[14] Elabd, R. H. and H. H. Abdullah, "A high isolation UWB MIMO vivaldi antenna based on CSRR-NL for contemporary 5G millimeter-wave applications," *Journal of Infrared, Millimeter, and Terahertz Waves*, Vol. 43, No. 11, 920–941, 2022.

[15] Kissi, C., M. Särestöniemi, T. Kumpuniemi, M. Sonkki, S. Myllymäki, M. N. Srifi, and C. Pomalaza-Raez, "Directive low-band UWB antenna for in-body medical communications," *IEEE Access*, Vol. 7, 149 026–149 038, 2019.

[16] Tang, Z., X. Wu, J. Zhan, S. Hu, Z. Xi, and Y. Liu, "Compact UWB-MIMO antenna with high isolation and triple band-notched characteristics," *IEEE Access*, Vol. 7, 19 856–19 865, 2019.

[17] Elabd, R. H. and A. J. A. Al-Gburi, "SAR assessment of miniaturized wideband MIMO antenna structure for millimeter wave 5G smartphones," *Microelectronic Engineering*, Vol. 282, 112098, 2023.

[18] Marzouk, M., I. H. Nejdi, Y. Rhazi, and M. Saih, "Multiband and wide band octagonal fractal antenna for telecommunication applications," in *2022 8th International Conference on Optimization and Applications (ICOA)*, 1–6, Genoa, Italy, Oct. 2022.

[19] Benkhadda, O., M. Saih, S. Ahmad, A. J. A. Al-Gburi, Z. Zakaria, K. Chaji, and A. Reha, "A miniaturized tri-wideband sierpinski hexagonal-shaped fractal antenna for wireless communication applications," *Fractal and Fractional*, Vol. 7, No. 2, 115, 2023.

[20] Oraizi, H. and S. Hedayati, "Miniaturization of microstrip antennas by the novel application of the giuseppe peano fractal geometries," *IEEE Transactions on Antennas and Propagation*, Vol. 60, No. 8, 3559–3567, 2012.

[21] Tripathi, S., A. Mohan, and S. Yadav, "Hexagonal fractal ultra-wideband antenna using Koch geometry with bandwidth enhancement," *IET Microwaves, Antennas & Propagation*, Vol. 8, No. 15, 1445–1450, 2014.

[22] Manikandan, P., P. Sivakumar, K. S. V. Krishna, P. Sumanth, and T. Poornesh, "A fractal based CSRR loaded multi-band antenna for wireless applications," *International Journal of Advance Science and Technology*, Vol. 29, No. 7s, 4486–4492, 2020.

[23] Manohar, M., "Miniaturised low-profile super-wideband Koch snowflake fractal monopole slot antenna with improved BW and stabilised radiation pattern," *IET Microwaves, Antennas & Propagation*, Vol. 13, No. 11, 1948–1954, 2019.

[24] Desai, A., T. K. Upadhyaya, R. Patel, S. Bhatt, and P. Mankodi, "Wideband high gain fractal antenna for wireless applications," *Progress In Electromagnetics Research Letters*, Vol. 74, 125–130, 2018.

[25] Kantharia, M., A. Desai, T. K. Upadhyaya, R. Patel, P. Mankodi, and M. Kantharia, "High gain flexible CPW fed fractal antenna for Bluetooth/WLAN/WPAN/WiMAX applications," *Progress In Electromagnetics Research Letters*, Vol. 79, 87–93, 2018.

[26] Marzouk, M., I. H. Nejdi, Y. Rhazi, and M. Saih, "Multiband and wide band octagonal fractal antenna for telecommunication applications," in *2022 8th International Conference on Optimization and Applications (ICOA)*, 1–6, 2022.

[27] Nejdi, I. H., S. Bri, M. Marzouk, S. Ahmad, Y. Rhazi, M. A. Lafkih, Y. A. Sheikh, A. Ghaffar, and M. Hussein, "UWB circular fractal antenna with high gain for telecommunication applications," *Sensors*, Vol. 23, No. 8, 4172, 2023.

[28] Marzouk, M., Y. Rhazi, I. H. Nejdi, F.-E. Zerrad, M. Saih, S. Ahmad, A. Ghaffar, and M. Hussein, "Ultra-wideband compact fractal antenna for WiMAX, WLAN, C and X band applications," *Sensors*, Vol. 23, No. 9, 4254, 2023.

[29] Sran, S. S. and J. S. Sivia, "ANN and IFS based wearable hybrid fractal antenna with DGS for S, C and X band application," *AEU — International Journal of Electronics and Communications*, Vol. 127, 153425, 2020.

[30] Werner, D., M. Gregory, Z. H. Jiang, and D. E. Brocker, "Optimization methods in antenna engineering," *Handbook of Antenna Technologies*, 321–376, Springer Singapore, 2016.

[31] Verma, R. K. and D. K. Srivastava, "Design, optimization and comparative analysis of T-shape slot loaded microstrip patch antenna using PSO," *Photonic Network Communications*, Vol. 38, 343–355, 2019.

[32] Fan, X., Y. Tian, and Y. Zhao, "Optimal design of multiband microstrip antennas by self-renewing fitness estimation of particle swarm optimization algorithm," *International Journal of Antennas and Propagation*, Vol. 2019, 1–9, 2019.

[33] D'Orazio, L., "Study and development of novel techniques for PHY-layer optimization of smart terminals in the context of next-generation mobile communications," Ph.D. dissertation, University of Trento, Trento, Italy, 2008.

[34] Ni, L. and S. Du, "Evolutionary particle swarm algorithm based on higher order cumulant fitting for blind channel identification," in *2008 4th International Conference on Wireless Communications, Networking and Mobile Computing*, 2008.

[35] Wang, Q., J. Zhang, and J. Yang, "Identification of nonlinear communication channel using an novel particle swarm optimization technique," in *2008 International Conference on Computer Science and Software Engineering*, Vol. 1, 1162–1165, Dec. 2008.

[36] Shami, T. M., A. A. El-Saleh, M. Alswaitti, Q. Al-Tashi, M. A. Summakieh, and S. Mirjalili, "Particle swarm optimization: A comprehensive survey," *IEEE Access*, Vol. 10, 10 031–10 061, 2022.

[37] Song, C., L. Pan, Y. Jiao, and J. Jia, "A high-performance transmitarray antenna with thin metasurface for 5G communication based on PSO (particle swarm optimization)," *Sensors*, Vol. 20, No. 16, 4460, 2020.

[38] Kang, M.-S., Y.-J. Won, B.-G. Lim, and K.-T. Kim, "Efficient synthesis of antenna pattern using improved PSO for spaceborne SAR performance and imaging in presence of element failure," *IEEE Sensors Journal*, Vol. 18, No. 16, 6576–6587, 2018.

[39] Khan, M. A., U. Rafique, H. S. Savci, A. N. Nordin, S. H. Kiani, and S. M. Abbas, "Ultra-wideband pentagonal fractal antenna with stable radiation characteristics for microwave imaging applications," *Electronics*, Vol. 11, No. 13, 2061, 2022.

[40] Sharma, N. and S. S. Bhatia, "Stubs and slits loaded partial ground plane inspired hexagonal ring-shaped fractal antenna for multiband wireless applications: Design and measurement," *Progress In Electromagnetics Research C*, Vol. 112, 99–111, 2021.

[41] Danjuma, I. M., M. O. Akinsolu, C. H. See, R. A. Abd-Alhameed, and B. Liu, "Design and optimization of a slotted monopole antenna for ultra-wide band body centric imaging applications," *IEEE Journal of Electromagnetics, RF and Microwaves in Medicine and Biology*, Vol. 4, No. 2, 140–147, 2020.

[42] Mahmood, S. N., A. J. Ishak, T. Saeidi, A. C. Soh, A. Jalal, M. A. Imran, and Q. H. Abbasi, "Full ground ultra-wideband wearable textile antenna for breast cancer and wireless body area network applications," *Micromachines*, Vol. 12, No. 3, 322, Mar. 2021.

[43] Subramanian, S., B. Sundarambal, and D. Nirmal, "Investigation on simulation-based specific absorption rate in ultra-wideband antenna for breast cancer detection," *IEEE Sensors Journal*, Vol. 18, No. 24, 10 002–10 009, 2018.

[44] Hussain, M., T. Islam, M. S. Alzaidi, D. H. Elkamchouchi, F. N. Alsunaydih, F. Alsaleem, and K. Alhassoon, "Single iterated fractal inspired UWB antenna with reconfigurable notch bands for compact electronics," *Heliyon*, Vol. 9, No. 11, 2023.

[45] Lasemi, Z. and Z. Atlasbaf, "Impact of fidelity factor on breast cancer detection," *IEEE Antennas and Wireless Propagation Letters*, Vol. 19, No. 10, 1649–1653, 2020.

[46] Puri, S. C., S. Das, and M. G. Tiary, "A multiband antenna using plus-shaped fractal-like elements and stepped ground plane," *International Journal of RF and Microwave Computer-Aided Engineering*, Vol. 30, No. 5, e22169, 2020.

[47] Marzouk, M., I. H. Nejdi, R. Youssef, S. Barua, S. Mohamed, S. Ahmad, and M. Hussein, "Efficient broadband fractal antenna for WiMAX and WLAN," *Heliyon*, Vol. 10, No. 5, 2024.